

Scaling properties and intermittency of two-dimensional turbulence in pure electron plasmas

F. Lepreti,^{1,*} M. Romé,² G. Maero,² B. Paroli,² R. Pozzoli,² and V. Carbone³

¹*Dipartimento di Fisica, Università della Calabria, and Consorzio Nazionale Interuniversitario per le Scienze Fisiche della Materia (CNISM), Unità di Cosenza, Ponte P. Bucci 31C, I-87036 Rende (CS), Italy*

²*Istituto Nazionale di Fisica Nucleare, Sezione di Milano and Dipartimento di Fisica, Università degli Studi di Milano, Via Celoria 16, I-20133 Milano, Italy*

³*Dipartimento di Fisica, Università della Calabria, and IPCF-CNR LiCryl Laboratory, Ponte P. Bucci 31C, I-87036 Rende (CS), Italy*
(Received 19 March 2013; published 20 June 2013)

When the cold nonrelativistic guiding center approximation is valid, the transverse dynamics of highly magnetized electron plasma columns confined in Penning-Malmberg traps is analogous to that of an incompressible, inviscid, two-dimensional (2D) fluid whose vorticity corresponds, up to a constant of proportionality, to the axially averaged electron plasma density. In this work intermittency phenomena in the freely decaying 2D electron plasma turbulence are investigated through scaling properties of the probability density functions and flatness of spatial vorticity increments, computed by analyzing the results of experiments performed in the Penning-Malmberg trap ELTRAP. It is shown that the intermittency properties of the turbulence strongly depends on the initial conditions and the relation of these results to the dynamics of the system is discussed.

DOI: [10.1103/PhysRevE.87.063110](https://doi.org/10.1103/PhysRevE.87.063110)

PACS number(s): 52.27.Jt, 47.27.De

I. INTRODUCTION

Highly magnetized, pure electron plasmas confined in Penning-Malmberg traps [1] can be used for experimental studies of two-dimensional (2D) fluid turbulence.

The electron motion in these traps is characterized by well separated time scales, i.e., the gyromotion period $\tau_c = 1/\nu_c$, with $\nu_c = eB/2\pi m$ the electron gyrofrequency, the axial bounce period $\tau_b = 2L/v_{th}$, the time scale of the transverse drift motion τ_d , and the collisional time scale τ_{coll} . Here, m and $-e$ are the electron mass and charge, respectively, B is the strength of the magnetic field (uniform and directed along the axis of the trap), L the trap length, and $v_{th} = (T/m)^{1/2}$ the thermal speed of the electrons, with T the plasma temperature. Under typical conditions of trapped electron plasma experiments (see next section), the ordering of the time scales is $\tau_c \ll \tau_b \ll \tau_d \ll \tau_{coll}$. The time average of the electron motion over cyclotron and bounce time scales corresponds to the 2D transverse dynamics of longitudinal electron columns.

Thus, operational conditions in such devices can be chosen in such a way that the cold nonrelativistic guiding center approximation is valid and the transverse dynamics of the electron plasma is well described by the drift-Poisson equations [2,3],

$$\frac{\partial n}{\partial t} + \mathbf{v} \cdot \nabla n = 0, \quad (1)$$

$$\mathbf{v} = -\frac{\nabla\phi \times \mathbf{B}}{B^2}, \quad (2)$$

$$\nabla^2\phi = \frac{en}{\epsilon_0}, \quad (3)$$

where n is the electron density, \mathbf{v} the electric drift velocity, ϕ the electrostatic potential, and ϵ_0 the vacuum permittivity. These equations are isomorphic to the Euler equations for an ideal (incompressible, inviscid) 2D fluid with vorticity

$\zeta = en/\epsilon_0 B$ and stream function $\psi = \phi/B$. With respect to other systems used to investigate 2D flows, e.g., rotating tanks [4], soap films [5], electrolyte layers [6,7], electron plasmas provide the possibility to significantly reduce nonideal effects, as no boundary layer exists, free-slip boundary conditions hold, the velocity field is divergence-free, and viscosity effects are almost negligible when the plasma is confined under ultrahigh vacuum conditions (residual gas pressure below 10^{-8} mbar).

There are, of course, limitations to the 2D fluid analogy. The most relevant effect is the occurrence of different drifts near the plasma edge, due to the finite width of the parallel velocity distribution. This problem has been first analyzed theoretically and experimentally in Ref. [8]. The result is that three-dimensional (3D) effects are negligible for all spatial structures with scales above a certain limit. In its simplest form this lower limit is λ_D^2/L where $\lambda_D = (\epsilon_0 T/e^2 n)^{1/2}$ is the Debye length. For the experiments reported in the present paper the resulting scale length limit is well below 0.1 mm, which is lower than the resolution of the optical diagnostics (see next section).

A further indication of the validity of the 2D approximation comes from numerical simulations. The transverse dynamics of a confined non-neutral plasma and in particular the formation and evolution of vortex structures in the 2D freely decaying turbulence has been investigated with a variety of approaches, e.g., particle-in-cell [9–12], fluid-Vlasov [13,14], contour dynamics [15,16] simulations have been performed, showing an excellent agreement with experiments. Extensions of such methods have also been used to investigate the transition to 3D regimes [17,18].

The free evolution of the system is typically characterized by the rapid formation of a high number of small vortices, which then interact through close encounters resulting in merger events and emission of vorticity filaments, leading eventually to the formation of a diffuse background. The plasma tends to reach an equilibrium state, characterized by a monotonically decreasing radial density profile, in which all the small-scale structures are smeared out. This typical

*fabio.lepreti@fis.unical.it

relaxation is sometimes halted when individual strong vortices settle into a stable, rotating “crystal-like” pattern [19–21], with a lifetime of hundreds of periods of the azimuthal plasma rotation. A final azimuthally symmetric equilibrium state is eventually reached through dissipative processes on a collisional time scale. Different theories have been developed in order to characterize the free relaxation of 2D turbulence. Variational principles based on either minimization of enstrophy (see, e.g., [22–24]) or maximization of entropy (see, e.g., [14,25–27]) have been used to describe the evolution towards relaxed states. In the so-called punctuated scaling theory [28,29], the turbulent flow is assumed to be dominated by well-separated strong vortices (following the Hamiltonian dynamics of point vortices), “punctuated” by occasional mergers of like-sign vortices. In order to characterize the vortex crystal states, Jin and Dubin [30,31] developed the so-called “regional” maximum fluid entropy theory. According to this theory, the strong coherent vortices present in the flow ergodically mix the background, which in turn affects the dynamics of the strong vortices, “cooling” their chaotic motion and driving them into an equilibrium pattern.

The scaling properties of 2D turbulence in electron plasmas have been investigated in the last years through different approaches. Kawai *et al.* [32] performed a spectral analysis based on the Fourier transform and confirmed the inverse energy and direct enstrophy cascades expected from classical theories [33,34]. They also reported power law spectra $E(k) \propto k^{-\alpha}$ in the enstrophy cascade range with exponents between 3.5 and 5.2, larger than the expected value $\alpha = 3$ and attributed this discrepancy to the effect of the long persistence of high-vorticity patches. Kawai and Kiwamoto [35] applied wavelet transforms [36] to show that this allows one to effectively discriminate the instrumental noise and to analyze the scaling behavior of the electron density fluctuations. In [37] the wavelet spectra for the coherent and the incoherent parts of the flow of both enstrophy and energy were obtained. It was found that the incoherent component does not contribute significantly to the dynamical properties of the 2D electron plasma flow, and is characterized by a near Gaussian probability density function (PDF) of the vorticity and by an increasing spatial wave-number spectrum. The wavelet spectral analysis of the coherent part of the flow instead evidenced that most of the enstrophy is contained at spatial scales of the order of $\simeq 5$ mm, corresponding to the typical size of the persistent vortices in the flow.

The dynamics of the freely decaying 2D turbulence in electron plasmas has been recently studied [38] by applying the proper orthogonal decomposition (POD) [39] to the results of experiments performed in the Penning-Malmberg device ELTRAP [40]. The POD is generally used to identify coherent structures and describe their contribution to the dynamics of the system. The technique provides a basis of functions for the mode decomposition of an ensemble of observations obtained from experiments (or numerical simulations). The POD analysis of electron plasma 2D turbulence enabled one to identify the coherent structures which give the dominant contribution to the plasma turbulent evolution, starting from different initial conditions for the electron density.

This work focuses on the intermittency phenomena associated with the 2D turbulence in pure electron plasmas.

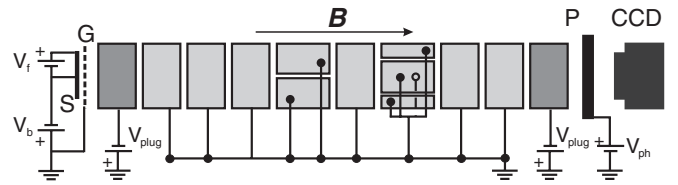


FIG. 1. Schematic of the Penning-Malmberg trap ELTRAP. The inner cylinders are grounded, while a (negative) potential V_{plug} is applied to the end plugs. A uniform magnetic field B is directed along the axis of the trap. The electron source (S) on the left is a spiral thermionic cathode, biased at a negative voltage V_b with respect to a grounded grid (G). The voltage drop across the filament is denoted by V_f . The optical diagnostics on the right comprises a phosphor screen (P) biased at a high positive potential V_{ph} and a CCD camera (activated by an external trigger synchronized with the dump of the plasma).

These phenomena are investigated by analyzing the results of experimental sequences obtained in ELTRAP, similar to those used for the POD analysis. The characterization of the intermittency is performed by analyzing the scaling properties of vorticity increments’ statistics by means of the PDFs and the flatness. The dependence of the intermittency properties of the 2D electron plasma turbulence on the initial conditions has not been previously studied in the literature.

The article is organized as follows. The experiments are described in Sec. II. The data analysis techniques and the results are presented in Sec. III. Section IV is devoted to conclusions.

II. EXPERIMENTS

The experimental results reported in the present paper on the formation and the evolution of coherent structures in an electron plasma have been obtained in the Penning-Malmberg trap ELTRAP. A scheme of the experimental apparatus is shown in Fig. 1. The electrons are contained in a set of cylindrical electrodes, with internal radius $R_W = 4.5$ cm. Eight electrodes have a length of 9 cm and two electrodes

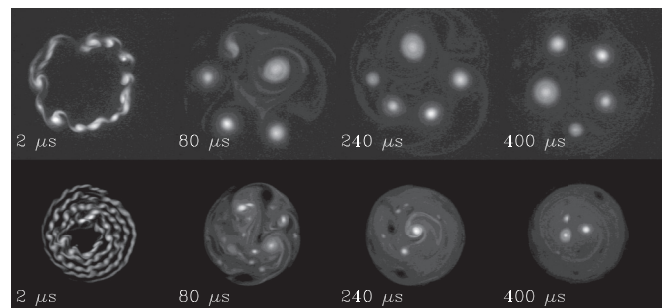


FIG. 2. Snapshots of the plasma density for the two analyzed sequences. (Top row) Experimental sequence with an annular initial density profile. The potentials of the cathode source are $V_b = 0.8$ V and $V_f = -4.1$ V. (Bottom row) Experimental sequence with a spiral initial density profile. The potentials of the cathode source are $V_b = -15$ V and $V_f = -3.6$ V. The trapping time is indicated at the bottom left corner of each frame. For both sequences the magnetic field is $B = 0.117$ T and the residual neutral gas pressure is $p \simeq 3 \times 10^{-9}$ mbar.

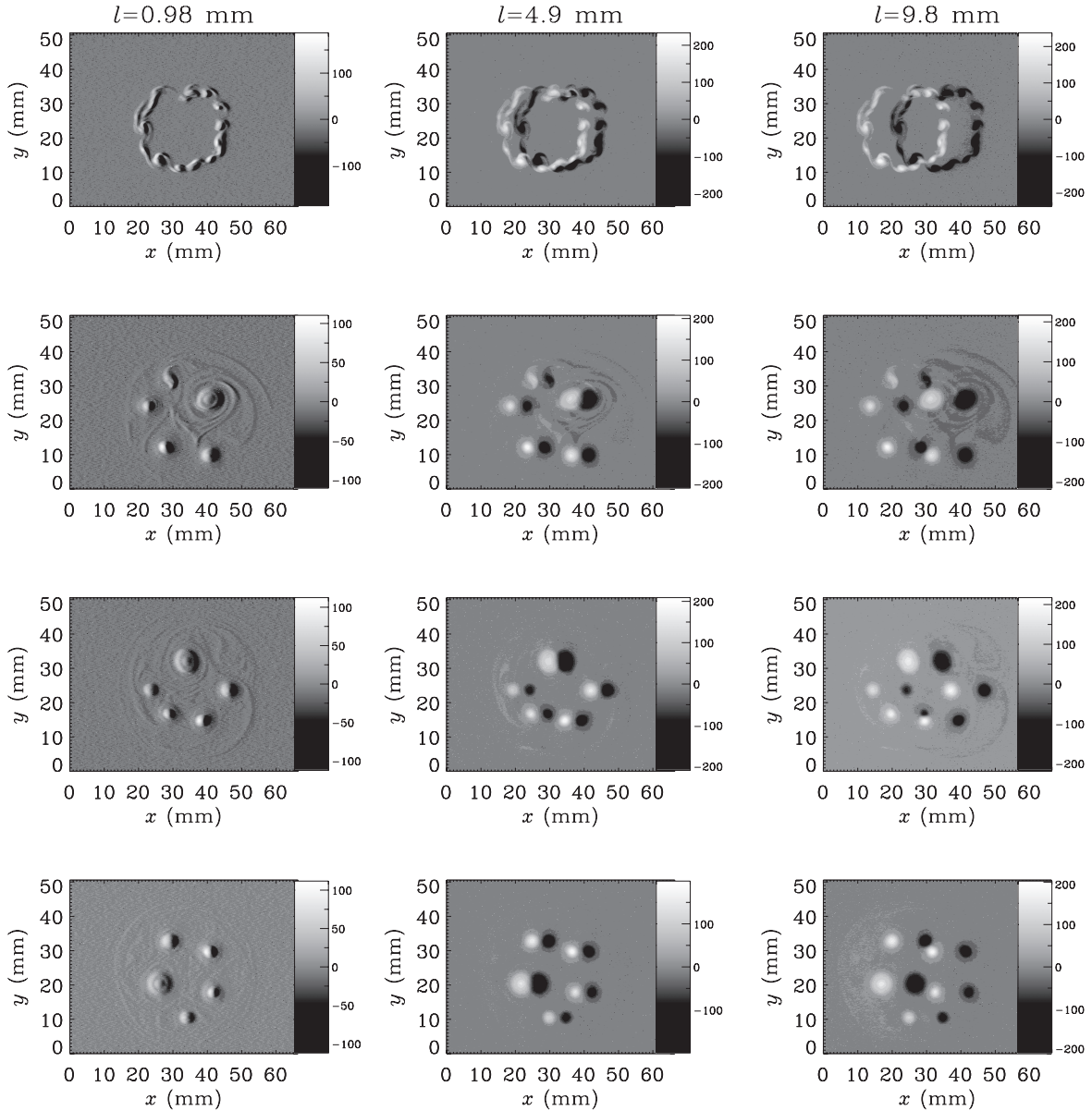


FIG. 3. Contour plots of the vorticity increments $\Delta\zeta_l^{(x)}(x, y)$ (grayscale bars, arbitrary units) for annular initial conditions, trapping times of $t = 2 \mu\text{s}$ (first row), $t = 80 \mu\text{s}$ (second row), $t = 240 \mu\text{s}$ (third row), $t = 400 \mu\text{s}$ (fourth row), and for different spatial separations l : $l = 0.98 \text{ mm}$ (left column), $l = 4.9 \text{ mm}$ (center column), $l = 9.8 \text{ mm}$ (right column). The coordinates of the trap axis are $x = 35 \text{ mm}$ and $y = 24 \text{ mm}$.

with length 15 cm are divided into two and four electrically isolated azimuthal sectors, respectively. They can be used for active manipulation and control of plasma rotation and shape [41–43].

A strong uniform magnetic field (up to 0.2 T) provides the Lorentz force for radial confinement of the plasma, while the axial confinement is provided by a suitable negative potential (typical value -100 V) applied on two cylinders. The apparatus is operated in an inject–hold-and-manipulate–dump cycle, and the time evolution of the system is monitored by means of an optical diagnostic system. During the injection stage the cylinder close to the electron source (plug-in electrode) is briefly grounded, allowing electrons emitted from the source to enter into the trap. The electrons are axially repelled by a potential applied to a second cylinder

(plug-out electrode). The plasma is then separated from the source by means of a potential applied to the plug-in electrode.

The confined plasma is diagnosed by detecting the time evolution of the charge induced on different cylindrical electrodes between the end plugs [44]. Plasma columns with a length $L_P = 10\text{--}80 \text{ cm}$, and a radius $R_P \lesssim 2.0 \text{ cm}$ can be confined, with an electron density $n = 10^6\text{--}10^7 \text{ cm}^{-3}$ and a temperature $T = 1\text{--}10 \text{ eV}$. The characteristic length scales of the system are the gyroradius $\rho_L = v_{\text{th}}/\omega_c \approx 50\text{--}500 \mu\text{m}$ and the Debye length $\lambda_D \approx 0.25\text{--}1 \text{ cm}$. The characteristic frequencies are the cyclotron frequency $\nu_c \approx 0.5\text{--}5 \text{ GHz}$, the plasma frequency $\omega_p/2\pi = (ne^2/\epsilon_0 m)^{1/2}/2\pi \approx 10\text{--}25 \text{ MHz}$, the axial bounce frequency $\nu_b \approx 0.5\text{--}5 \text{ MHz}$, and the azimuthal rotation frequency of the plasma $\nu_d \approx 10\text{--}200 \text{ kHz}$.

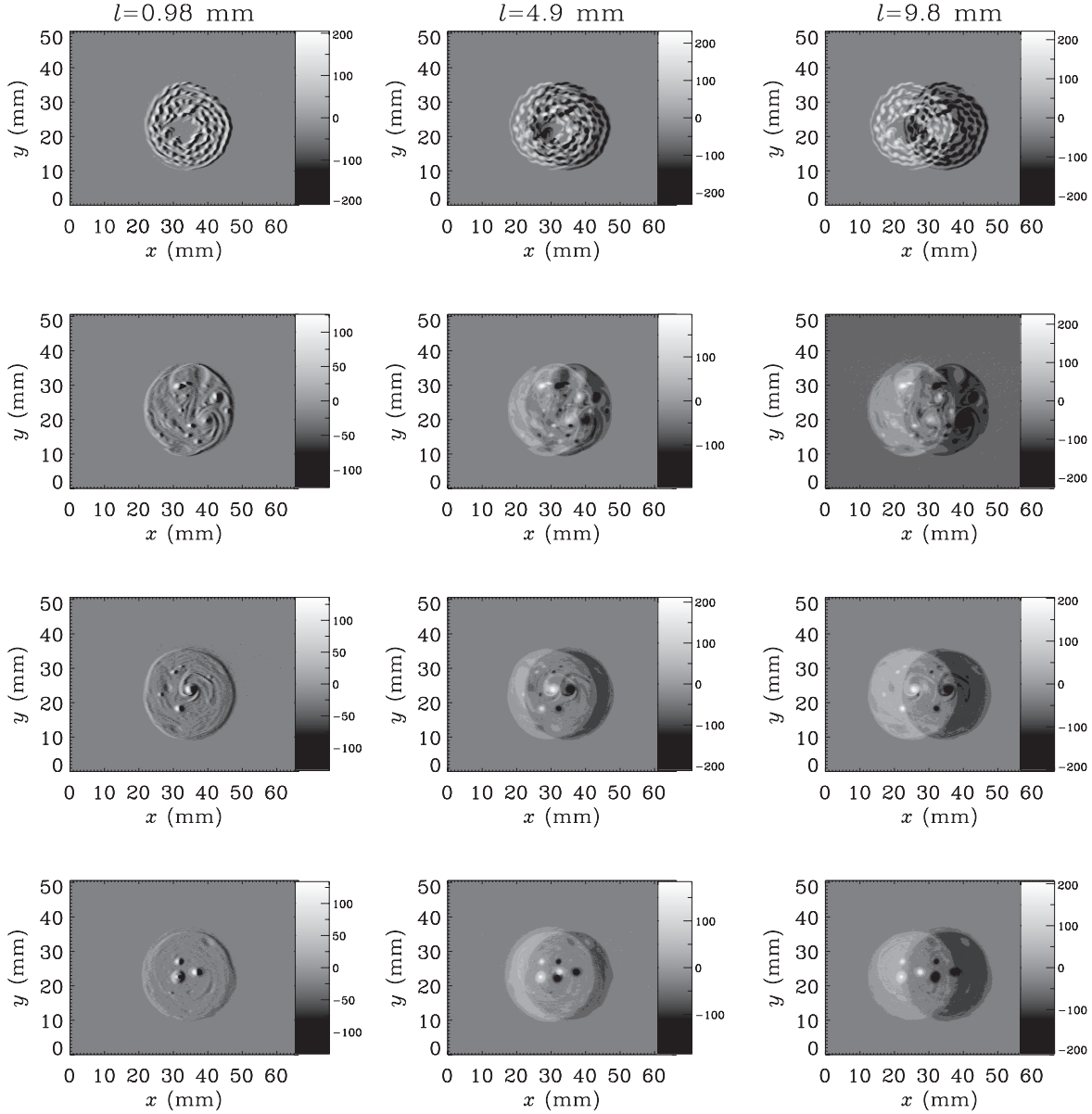


FIG. 4. The same as in Fig. 3 for spiral initial conditions.

After a given confinement time, the plug-out electrode is grounded and the electrons are dumped onto a phosphor screen kept at a high positive voltage (10–15 kV). The resulting light is imaged with a triggered CCD camera. The intensity of the light in each point on the snapshot is proportional to the axially averaged plasma density $n(x,y,t)$, with (x,y) Cartesian coordinates in the plane transverse to the magnetic field. The CCD camera has a resolution of 1376×1035 pixels and a signal-to-noise ratio of 63 dB. In all images reported in this paper the spatial resolution is $\simeq 50 \mu\text{m}/\text{pixel}$. The optical measurement destroys the plasma, so that each image is actually obtained with a different plasma. However, the shot-to-shot reproducibility of the initial conditions is very high (the maximum relative variation of the measured charge at a given time is typically less than 0.1%), so that the transverse dynamics of the plasma can be accurately reconstructed by keeping the injection parameters fixed and increasing the trapping (hold) time.

The electrons are thermally emitted by a spirally wound thoriated tungsten filament (with a diameter of 2.54 cm) [45], heated with a constant current and biased with respect to a grounded grid (see Fig. 1). The potential varies as $V_k(r) = V_b + V_f(r/R_k)^2$, where R_k is the radius of the cathode, V_b is the bias potential applied to the center of the cathode, and V_f is the potential drop between the ends of the cathode [1] (see Fig. 1). By adjusting V_b and V_f , different initial spatial distributions of the electrons can be obtained.

The experimental sequences consist of $N = 250$ frames with a trapping time step of $2 \mu\text{s}$. The total duration is much smaller than the electron-electron and electron-neutral collision times, which are both a few tens of ms for the experimental parameters used here. The plasma density evolution for the sequences considered in the rest of the paper is shown in Fig. 2. The first frame in both sequences (corresponding to a trapping time $\tau = 2 \mu\text{s}$) reflects the shape of the initial density distribution. The diocotron

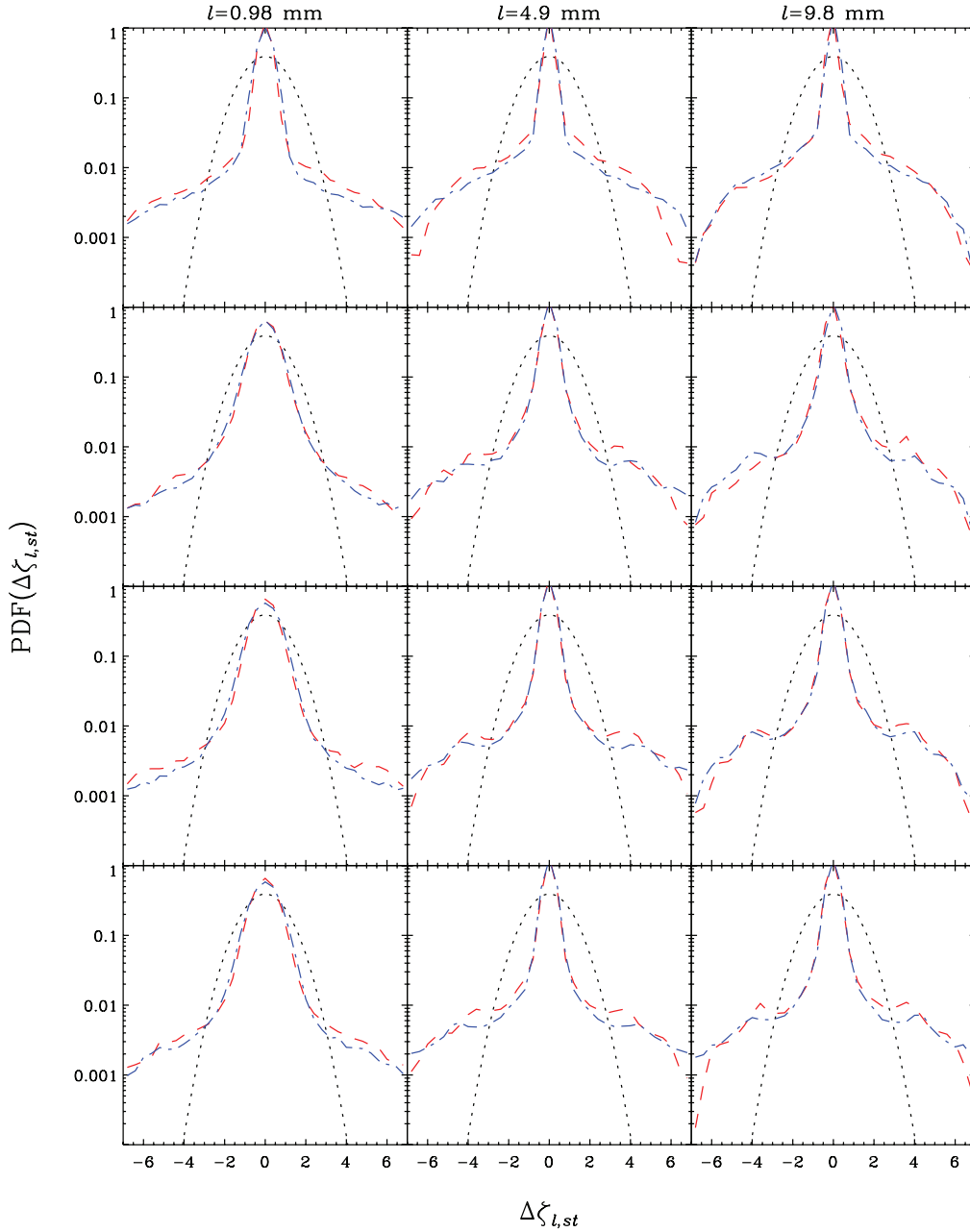


FIG. 5. (Color online) PDFs of the normalized vorticity increments $\Delta\zeta_{l,st}$ along the x (red dashed lines) and y (blue dash-dotted lines) directions for annular initial conditions, trapping times of $t = 2 \mu\text{s}$ (first row), $t = 80 \mu\text{s}$ (second row), $t = 240 \mu\text{s}$ (third row), $t = 400 \mu\text{s}$ (fourth row), and for different spatial separations l : $l = 0.98 \text{ mm}$ (left column), $l = 4.9 \text{ mm}$ (center column), $l = 9.8 \text{ mm}$ (right column). The Gaussian PDFs with zero mean and $\sigma = 1$ are also shown for comparison (dotted curves).

(Kelvin-Helmholtz) instability rapidly leads to a nonlinear evolution of the flow and to the development of turbulence. Two types of initial conditions for the electron density, namely annular and spiral configurations, have been considered (the former case corresponds to $-V_f > V_b > 0$).

III. DATA ANALYSIS AND RESULTS

One of the fundamental tools to study the properties of turbulent flows is the analysis of the statistics of field increments (also field differences) calculated across different scale separations. This provides information about intermit-

tency phenomena and presence of coherent structures such as vortices, filaments, and shocks. For a turbulent field $u(\mathbf{r}, t)$ the increments across a scale separation l are defined as $\Delta u_l(\mathbf{r}, t) = u(\mathbf{r} + l, t) - u(\mathbf{r}, t)$. In this work, the properties of the 2D vorticity $\zeta(x, y, t)$ are of interest. The spatial increments of vorticity $\Delta\zeta_l^{(x)}(x, y, t)$ and $\Delta\zeta_l^{(y)}(x, y, t)$ in both x and y directions are considered, namely

$$\Delta\zeta_l^{(x)}(x, y, t) = \zeta(x + l, y, t) - \zeta(x, y, t), \quad (4)$$

$$\Delta\zeta_l^{(y)}(x, y, t) = \zeta(x, y + l, t) - \zeta(x, y, t). \quad (5)$$

The vorticity increments $\Delta\zeta_l^{(x)}(x, y)$ along the x direction for three values of the separation l and at four time instants during the plasma evolution (the same as those considered in Fig. 2) are shown in Fig. 3 for the annular initial condition and in Fig. 4 for the spiral initial condition. The increments $\Delta\zeta_l^{(y)}(x, y)$ are not shown as they have similar patterns.

In order to investigate the scaling properties of the statistics of vorticity increments, the PDFs and the flatness function are computed. These statistical methods have been applied extensively to analyze turbulence in fluids (see, e.g., [46] and references therein) and in plasmas (see, e.g., [47,48] and references therein).

A first picture of how the vorticity increments' statistics change with the scale l can be obtained by looking at the increments' PDFs for different l values. In fact, one of the signatures of intermittency is the change of the PDF shape with the scale l . In order to compare in an effective way the shape of the PDFs at different scales, normalized increments are used, defined as

$$\Delta\zeta_{l,st} = \frac{\Delta\zeta_l - \langle\Delta\zeta_l\rangle}{\sigma_{\Delta\zeta_l}}, \quad (6)$$

where $\langle\Delta\zeta_l\rangle$ and $\sigma_{\Delta\zeta_l}$ are the mean value and the standard deviation of $\Delta\zeta_l$, respectively.

More quantitative information about the scaling properties of field increments in turbulent flows can be obtained from the analysis of the so-called structure functions $S_p(l)$, which are defined as the moments of field increments, that is, $S_p(l) = \langle\Delta\zeta_l^p\rangle$, where $\langle\cdot\rangle$ denotes in this case spatial averages. Intermittency may be quantified by means of the flatness $F(l)$, which is defined as the ratio of the fourth-order moment to the square of the second-order moment,

$$F(l) = \frac{S_4(l)}{[S_2(l)]^2}. \quad (7)$$

The flatness is 3 for Gaussian PDFs, while in the presence of intermittency $F(l)$ increases as l decreases [46].

In the rest of this section the results obtained by the application of these statistical methods to both sequences shown in Fig. 2 are described. Several experimental sequences have been recorded for both sets of initial conditions. The data analysis yields results very close to those reported here.

The PDFs of the vorticity increments for the annular initial condition are shown in Fig. 5 for three values of the separation l and at four time instants during the plasma evolution. Already at $t = 2 \mu\text{s}$, i.e., very close to the initial condition, the PDFs show a central core and large increment tails at all spatial separations. It has been verified that the core, which is nearly Gaussian, corresponds to background fluctuations, while the tails are due to differences between high density values in the structures and low density values in the background. The PDFs show very little evolution over time. The only somewhat clear change occurs at small scales ($l = 0.98 \text{ mm}$) and it consists in a slight broadening of the central core.

The flatness of the vorticity increments along the x and y directions for the annular initial condition is shown in Fig. 6 for different trapping times. $F(l)$ grows as l decreases down to $l \approx 2 \text{ mm}$, but it does not change significantly with time, as

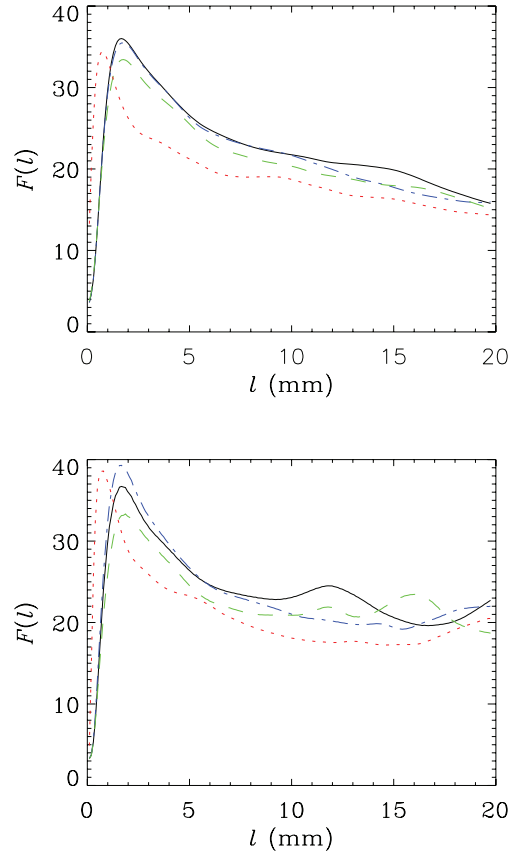


FIG. 6. (Color online) Flatness of the vorticity increments along the x (top) and y (bottom) directions for the annular initial condition and for different trapping times: $2 \mu\text{s}$ (red dotted lines), $80 \mu\text{s}$ (green dashed lines), $240 \mu\text{s}$ (blue dash-dotted lines), $400 \mu\text{s}$ (black solid lines).

already seen for the PDFs. Therefore, the growth of $F(l)$ is not due to the intermittency produced by the turbulent dynamics, but can be attributed to the shape of the initial condition. The noise of the optical diagnostics (see previous section) may affect the statistical analysis of the field increments at small spatial scales. This explains the decrease of $F(l)$ to the Gaussian value 3 observed for $l < 2 \text{ mm}$. In [35] the statistics of vorticity fluctuations for a sequence with annular initial condition was analyzed by means of wavelet transforms. It was found that the wavelet coefficients' flatness shows only slight systematic changes during the plasma evolution, in qualitative agreement with the results shown here.

The results are quite different for the case of spiral initial conditions. The PDFs (see Fig. 7) are nearly Gaussian at all the considered separations for $t = 2 \mu\text{s}$. However, in contrast with the previous case, a clear PDF evolution is found. As the time increases, tails at large increments appear and become stronger and stronger, especially at small spatial separations. The deviation from the Gaussian shape increases going from large to small scales, which indicates the occurrence of intermittency in the turbulent dynamics.

This is confirmed by the flatness $F(l)$ of the vorticity increments (see Fig. 8). $F(l) \approx 3$ at all scales for $t = 2 \mu\text{s}$, i.e., the vorticity fluctuations are Gaussian, as it could be expected from the PDF shapes. As the plasma evolves, the flatness starts

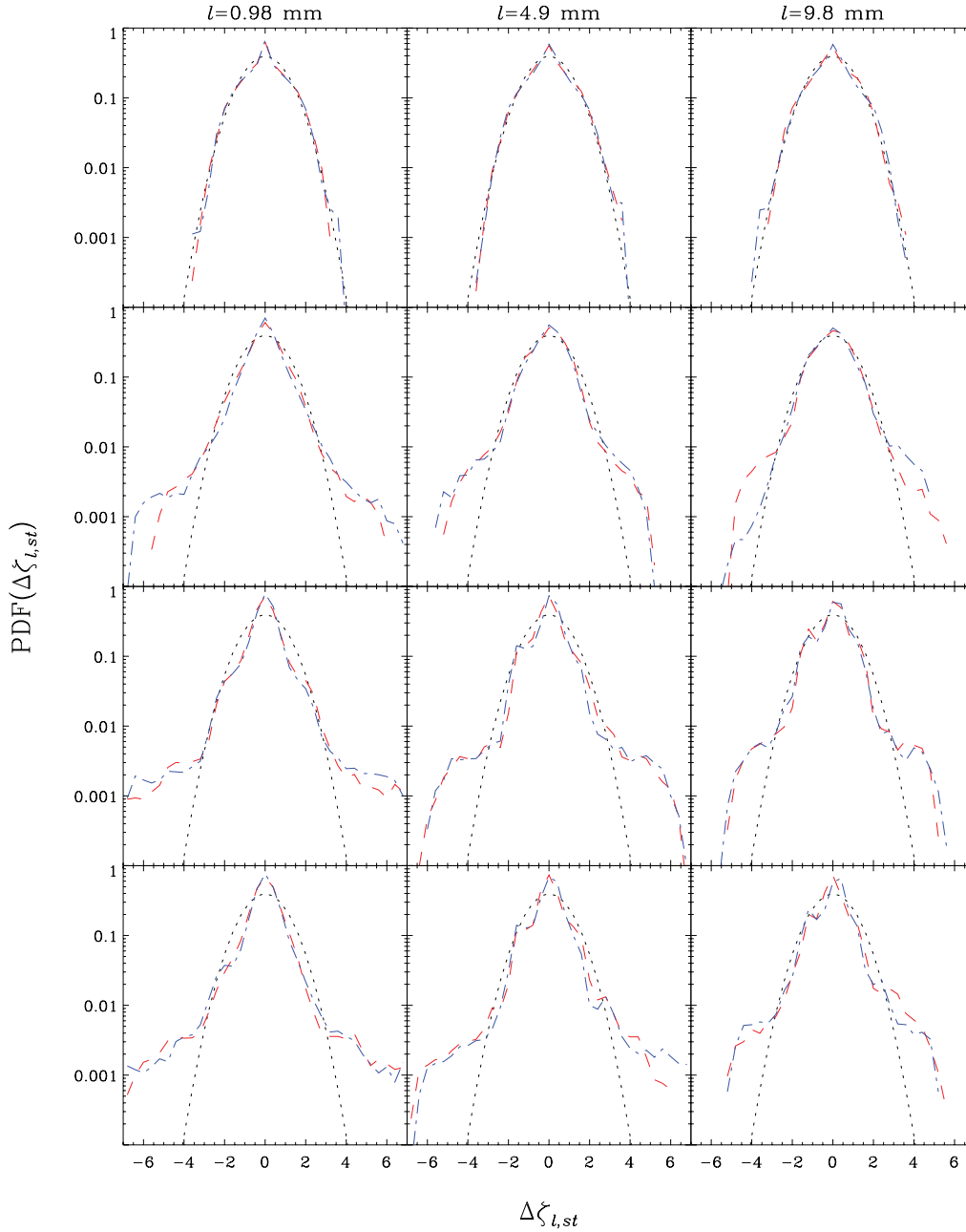


FIG. 7. (Color online) The same as in Fig. 5 for spiral initial conditions.

to grow going from large to small scales, down to $l \approx 1$ mm, and this growth is found to become stronger and stronger with time. Therefore, at variance with the annular case, the observed increase of the flatness at small scales is not a trivial effect already present in the initial conditions, but it represents the manifestation of the intermittency arising from the turbulent dynamics of the plasma. The decrease of the flatness to the Gaussian value 3 for $l < 1$ mm can be attributed also in this case to the instrumental noise fluctuations.

IV. CONCLUSIONS

In this work, the statistical and scaling properties of 2D turbulence in pure electron plasmas have been investigated

by analyzing the results of experiments carried out with the Penning-Malmberg device ELTRAP. A comparison between two types of initial conditions for the electron density, namely annular and spiral configurations, has been performed. The study focuses on the intermittency phenomena associated with the turbulent dynamics and is based on the analysis of scaling properties of vorticity increments' statistics by means of PDFs and flatness.

For the case of annular initial conditions it is found that the statistics of the vorticity increments does not change significantly during the plasma evolution. The scaling behavior of the increments is basically determined by the initial conditions and the plasma dynamics does not produce intermittency effects expected from a developed turbulent cascade.

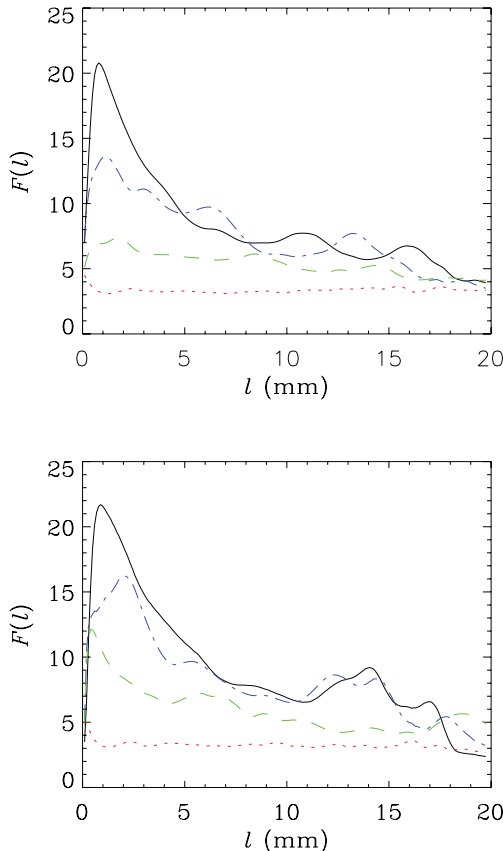


FIG. 8. (Color online) The same as in Fig. 6 for spiral initial conditions.

On the other hand, for the case of spiral initial conditions the vorticity increments show nearly Gaussian statistics at all spatial scales during the very early stages of the plasma evolution, while the appearance of large increment tails in the PDFs and the growth of the flatness at small scales (both effects becoming stronger and stronger with time) indicate the development of intermittency arising from the plasma turbulent dynamics.

In previous works [32,35,37] the analysis of the characteristics of the turbulent plasma evolution has been

performed starting from well-defined and quite similar initial conditions (namely, annular). Here we have performed a quantitative analysis of the intermittency properties, explicitly highlighting the strong dependence on the initial conditions. This dependence can be related to the dynamics underlying the system evolution. It has been suggested that annular initial conditions may lead to an evolution characterized by a low turbulence level [49], and this may prevent the occurrence of intermittency. It can be also useful to consider the POD analysis performed in [38] for experimental sequences similar to those studied here. The POD results indicate that for annular initial conditions the POD modes with the major enstrophy content are characterized by coherent structures of size 5–6 mm and time evolution with regular oscillations which can be attributed to the emergence of the fastest growing diocotron modes originating from the initial density annulus. For spiral initial conditions the POD analysis evidenced a more uniform enstrophy distribution among the POD modes and the coexistence of large-scale, coherent vortices and a background of smaller scale vorticity structures in a broader range of spatial scales. The time evolution of the mode coefficients was found to be dominated by stochastic fluctuations, indicating the presence of a fairly developed turbulent cascade process which gives rise to the intermittency phenomena evidenced in the present work.

The results of the analysis reported here suggest that a systematic investigation of the initial density conditions should be performed in order to characterize the parameters playing a major role in the early dynamics of the flow and leading to an evolution dominated either by the presence of coherent structures (and possibly the formation of vortex crystal-like states) or by a higher turbulence level. In this context, it is to be noted that studies concerning the early system dynamics are outside of the field of investigation of statistical theories, which typically rely on the presence of global constraints.

ACKNOWLEDGMENTS

This work was supported by the Italian Ministry for University and Research (MIUR) “PRIN 2009” funds (Grant No. 20092YP7EY).

-
- [1] J. H. Malmberg and J. S. deGrassie, *Phys. Rev. Lett.* **35**, 577 (1975).
 - [2] R. H. Levy, *Phys. Fluids* **8**, 1288 (1965).
 - [3] C. F. Driscoll and K. S. Fine, *Phys. Fluids B* **2**, 1359 (1990).
 - [4] C. N. Baroud, B. B. Plapp, Z. S. She, and H. L. Swinney, *Phys. Rev. Lett.* **88**, 114501 (2002).
 - [5] M. A. Rutgers, *Phys. Rev. Lett.* **81**, 2244 (1998).
 - [6] J. Paret and P. Tabeling, *Phys. Rev. Lett.* **79**, 4162 (1997).
 - [7] M. Rivera, P. Vorobieff, and R. E. Ecke, *Phys. Rev. Lett.* **81**, 1417 (1998).
 - [8] A. J. Peurrung and J. Fajans, *Phys. Fluids B* **5**, 4295 (1993).
 - [9] D. A. Schecter, D. H. E. Dubin, K. S. Fine, and C. F. Driscoll, *Phys. Fluids* **11**, 905 (1999).
 - [10] M. Amoretti, D. Durkin, J. Fajans, R. Pozzoli, and M. Romé, *Phys. Plasmas* **8**, 3865 (2001).
 - [11] G. Delzanno, G. Lapenta, and J. Finn, *IEEE Trans. Plasma Sci.* **30**, 34 (2002).
 - [12] K. Gomberoff, J. Fajans, J. Wurtele, A. Friedman, D. P. Grote, R. H. Cohen, and J.-L. Vay, *Phys. Plasmas* **14**, 052107 (2007).
 - [13] M. Romé, M. Brunetti, F. Califano, F. Pegoraro, and R. Pozzoli, *Phys. Plasmas* **7**, 2856 (2000).
 - [14] D. J. Rodgers, S. Servidio, W. H. Matthaeus, D. C. Montgomery, T. B. Mitchell, and T. Aziz, *Phys. Rev. Lett.* **102**, 244501 (2009).
 - [15] G. G. M. Coppa, F. Peano, and F. Peinetti, *J. Comput. Phys.* **182**, 392 (2002).
 - [16] G. Coppa, A. D’Angola, F. Peano, and F. Peinetti, *Eur. Phys. J. D* **26**, 275 (2003).
 - [17] Y. Tsidulko, R. Pozzoli, and M. Romé, *J. Comput. Phys.* **209**, 406 (2005).

- [18] E. N. Nikolaev, R. M. A. Heeren, A. M. Popov, A. V. Pozdnev, and K. S. Chingin, *Rapid Commun. Mass Spectrom.* **21**, 3527 (2007).
- [19] T. Havelock, *Philos. Mag.* **11**, 617 (1931).
- [20] L. Campbell and R. Ziff, Los Alamos Scientific Laboratory Report No. LA-7384-MS (1978).
- [21] K. S. Fine, A. C. Cass, W. G. Flynn, and C. F. Driscoll, *Phys. Rev. Lett.* **75**, 3277 (1995).
- [22] F. P. Bretherton and D. B. Haidvogel, *J. Fluid Mech.* **78**, 129 (1976).
- [23] W. H. Matthaeus and D. Montgomery, *Ann. N.Y. Acad. Sci.* **357**, 203 (1980).
- [24] X. P. Huang and C. F. Driscoll, *Phys. Rev. Lett.* **72**, 2187 (1994).
- [25] J. Miller, *Phys. Rev. Lett.* **65**, 2137 (1990).
- [26] R. Robert and J. Sommeria, *J. Fluid Mech.* **229**, 291 (1991).
- [27] J. Miller, P. B. Weichman, and M. C. Cross, *Phys. Rev. A* **45**, 2328 (1992).
- [28] G. F. Carnevale, J. C. McWilliams, Y. Pomeau, J. B. Weiss, and W. R. Young, *Phys. Rev. Lett.* **66**, 2735 (1991).
- [29] J. Weiss and J. McWilliams, *Phys. Fluids A* **5**, 608 (1993).
- [30] D. Z. Jin and D. H. E. Dubin, *Phys. Rev. Lett.* **80**, 4434 (1998).
- [31] D. Z. Jin and D. H. E. Dubin, *Phys. Rev. Lett.* **84**, 1443 (2000).
- [32] Y. Kawai, Y. Kiwamoto, Y. Soga, and J. Aoki, *Phys. Rev. E* **75**, 066404 (2007).
- [33] R. H. Kraichnan, *Phys. Fluids* **10**, 1417 (1967).
- [34] G. K. Batchelor, *Phys. Fluids* **12**, II-233 (1969).
- [35] Y. Kawai and Y. Kiwamoto, *Phys. Rev. E* **78**, 036401 (2008).
- [36] A. Grossmann and J. Morlet, *SIAM J. Math. Anal.* **15**, 723 (1984).
- [37] G. Bettega, R. Pozzoli, and M. Romé, *New J. Phys.* **11**, 053006 (2009).
- [38] M. Romé and F. Lepreti, *Eur. Phys. J. Plus* **126**, 38 (2011).
- [39] J. L. Lumley, in *Atmospheric Turbulence and Wave Propagation*, edited by A. M. Yaglom and V. I. Tatarski (Nauka, Moscow, 1967), p. 86.
- [40] M. Amoretti, G. Bettega, F. Cavaliere, M. Cavenago, F. D. Luca, R. Pozzoli, and M. Romé, *Rev. Sci. Instrum.* **74**, 3991 (2003).
- [41] G. Bettega, F. Cavaliere, B. Paroli, M. Cavenago, R. Pozzoli, and M. Romé, *Phys. Plasmas* **14**, 102103 (2007).
- [42] G. Bettega, F. Cavaliere, B. Paroli, R. Pozzoli, M. Romé, and M. Cavenago, *Phys. Plasmas* **15**, 032102 (2008).
- [43] G. Bettega, B. Paroli, R. Pozzoli, and M. Romé, *J. Appl. Phys.* **105**, 053303 (2009).
- [44] G. Bettega, B. Paroli, R. Pozzoli, M. Romé, and C. Svelto, *Meas. Sci. Technol.* **19**, 085703 (2008).
- [45] G. Bettega, F. Cavaliere, A. Illiberi, R. Pozzoli, M. Romé, M. Cavenago, and Y. Tsidulko, *Appl. Phys. Lett.* **84**, 3807 (2004).
- [46] U. Frisch, *Turbulence: The Legacy of A.N. Kolmogorov* (Cambridge University Press, Cambridge, 1995).
- [47] V. Carbone, F. Lepreti, L. Sorriso-Valvo, P. Veltri, V. Antoni, and R. Bruno, *Riv. Nuovo Cimento* **27**, 1 (2004).
- [48] R. Bruno and V. Carbone, *Living Rev. Solar Phys.* **2**, 4 (2005).
- [49] D. J. Rodgers, W. H. Matthaeus, T. B. Mitchell, and D. C. Montgomery, *Phys. Rev. Lett.* **105**, 234501 (2010).